AJNR

Revisiting the pathophysiology of intracranial hemorrhage in fetuses with Chiari II malformation – novel imaging biomarkers of disease severity?

Hui Shi, Daniela Prayer, Patric Kienast, Farjad Khalaveh, Johannes Tischer, Binder Julia, Michael Weber, Marlene Stuempflen and Gregor Kasprian

AJNR Am J Neuroradiol published online 7 May 2024
http://www.ajnr.org/content/early/2024/05/07/ajnr.A8331

ORIGINAL RESEARCH

Pediatric Neuroimaging

Revisiting the pathophysiology of intracranial hemorrhage in fetuses with Chiari II malformation – novel imaging biomarkers of disease severity?

Hui Shi, Daniela Prayer, Patric Kienast, Farjad Khalaveh, Johannes Tischer, Binder Julia, Michael Weber, Marlene Stuempflen, and Gregor Kasprian

ABSTRACT

BACKGROUND AND PURPOSE: Intracranial hemorrhage (ICH) has emerged as a notable concern in Chiari II malformation (CM II), yet its origins and clinical implications remain elusive. This study aims to validate the in-utero prevalence of ICH in CM II and investigate contributing factors, and visualize the findings in a network format.

MATERIALS AND METHODS: A single-center retrospective review of fetal MRI scans obtained in fetuses with CM II presenting (January 2007 to December 2022) was performed for ICH utilizing EPI-T2* blood-sensitive sequence. Fetuses with aqueduct stenosis (AS) were included as a control group. The incidence of ICH and corresponding gestational ages were compared between CM II and AS cases, and morphometric measurements (inner/outer CSF spaces, posterior fossa, venous structure) were compared among the four 1:1 age-matched groups: CM II+ICH, CM II-ICH, AS+ICH, and AS-ICH. Additionally, a co-occurrence network was constructed to visualize associations between phenotypic features in ICH cases.

RESULTS: A total of 101 fetuses with CM II and 90 controls with AS at a median gestational age of 24.4 weeks and 22.8 weeks(P=.138) were included. Prevalence of ICH in fetuses with CM II was higher compared to the AS cases (28.7% vs 18.9%, P=.023), accompanied by congested veins (deep vein congestion mainly in young fetuses, and cortical veins may also be affected in older fetuses). ICH was notably correlated with specific anatomical features, essentially characterized by reduced outer cerebrospinal fluid spaces and clivus-supraocciput angle. The co-occurrence network analysis reveals complex connections including bony defects, small posterior fossa dimensions, vermis ectopia, reduced CSF spaces as well as venous congestion and venous sinus stenosis as pivotal components within the network.

CONCLUSIONS: The high prevalence of ICH – detected by fetal MRI - among fetuses with CM emphasizes the pathophysiological importance of venous congestion, ICH, and vasogenic edema. As indicators of disease severity, these features may serve as helpful additional imaging biomarkers for the identification of potential candidates for fetal surgery.

ABBREVIATIONS: CM II = Chiari type II malformation; AS = aqueduct stenosis; ICH = Intracranial hemorrhage.

Received February 14, 2024; accepted after revision month day, year.
From the Department of Radiology (H.S.), Zhujiang Hospital, Southern Medical University, Guangzhou, China; Department of Biomedical Imaging and Image-guided Therapy (D.P., P.K., J.T., M.W., M.S., G.K.), Department of Neurosurgery (F.K.), and Department of Obstetrics and Feto-maternal Medicine (B.J.), Medical University of Vienna, Vienna, Austria.

The authors declare no conflicts of interest related to the content of this article.

Please address correspondence to Gregor Kasprian, MD, Department of Biomedical Imaging and Image-guided Therapy, Medical University of Vienna, Währinger Gürtel 18-20, Vienna, 1090, Austria; e-mail:gregor.kasprian@meduniwien.ac.at.

SUMMARY SECTION

PREVIOUS LITERATURE: Intracranial hemorrhage (ICH) is commonly detected by sonography and MR imaging in prenatal evaluation of Chiari II malformation (CM II) and is frequently described on postnatal MR imaging. Prenatal ICH is associated with prenatal and postnatal hindbrain herniation likely related to its close association with increased ventriculomegaly.

KEY FINDINGS: Vermis ectopia, skull remodeling, and altered CSF dynamics may result in dural sinus stenosis, venous congestion, and intracranial hypertension, which may contribute to ICH in CM II fetuses. Prenatal-identified ICH is correlated to more postnatal clinical morbidities and disabilities.

KNOWLEDGE ADVANCEMENT: With pathophysiological alterations underlying a more severe imaging phenotype in CM II, ICH in Chiari II fetuses should be considered imaging biomarkers for future neurological morbidity in prospective fetal surgery trials.

INTRODUCTION

Chiari II malformation(CM II), a primary disorder of segmentation of the embryonic neural tube into neuromeres[1], is often associated with hydrocephalus and aqueduct stenosis(AS). In addition to the spinal defect, this malformation is associated with a complex interplay of factors in the brain, including constriction of the posterior cranial fossa structures[2], ectopic vermis, impaired venous return [3], disturbed

Copyright 2024 by American Society of Neuroradiology.

CSF dynamics[3, 4]during fetal stage. This intricate relationship may create a vicious cycle [5], perpetuating the pathophysiological processes underlying this condition.

In previous studies, intracranial hemorrhage (ICH) has been identified as a notable concern in fetuses with CM II [6, 7], but its etiology remains unclear. Hindbrain herniation and its close association with ventriculomegaly were presumed potential contributing factors[6].

The presence of venous sinus stenosis [3] and "lemon head" characteristics in CM II suggests shared mechanisms with craniosynostosis[8] and Chiari I malformation[5, 9]. These parallels hint at common underlying factors affecting venous drainage. ICH could be a potential consequence of venous congestion/hypertension in CM II. However, specific imaging correlates between ICH and venous sinus alterations remain unexplored. A deeper understanding of these shared mechanisms could elucidate the clinical implications of ICH in CM II and influence prenatal surgical decision-making. In some institutions, ICH is even considered an exclusion criterion for surgery due to being deemed "unrelated to primary disease" [10].

In exploring the potential clinical significance of ICH in CM II fetuses, we aim to delve deeper into the underlying pathophysiology. Given the rarity of ICH occurrences in a normal cohort, we were seeking to use another condition with certain similarities to CM II to shed more light on the mechanism of ICH. By comparing the location and distinct features of ICH, CSF spaces, osseous architecture, and venous structure changes in another cohort characterized by hindered CSF circulation, we endeavor to elucidate whether obstructive hydrocephalus singularly accounts for hemorrhage, as hypothesized, or if additional factors contribute beyond the high stretch of the immature ependyma. Our study followed three primary objectives: validating the prevalence of brain hemorrhages in CM II through an extensive cohort analysis, exploring factors contributing to ICH based on morphometric measurement and a comparison to AS cases, and constructing a comprehensive model elucidating contributing factors utilizing co-occurrence network analysis.

MATERIALS AND METHODS

Participants

This retrospective single-center study was approved by the institutional internal review board (Ethics Committee number 1716/2017).

Inclusion criteria for the study were the presence of CM II – as characterized by the lemon configuration of the fetal head, small posterior fossa, cerebellar ectopia, kinking of the brain stem, and reduced external CSF spaces[1]. Due to the local center's long-standing history of fetal imaging, our database of over 8000 fetal MRI examinations between 1 January 2007 and 31 December 2022 was retrospectively evaluated and cases fulfilling the criteria of a Chiari II malformation were included in this study. Additionally, fetuses with congenital AS (presumed hemorrhagic/infection/genetic/ extrinsic occupied lesions) characterized by complete loss of aqueductal CSF signal at any level (obstruction), aqueduct funneling, enlarged inferior third ventricular recesses, enlargement of the lateral ventricles and third ventricle[11, 12], in conjunction with increased head circumference and/or cerebral size for gestational age, were incorporated as a control group. The flowchart of the included cases is presented in Figure 1.

Fetal MRI

In vivo fetal MRI was performed according to the ISUOG Practice Guidelines[13] using 1.5-T or a 3.0-T scanner (Philips Ingenia or Achieva with a 32-channel body coil; Philips Medical Systems). In each case, EPI-T2* weighted blood-sensitive sequence (TE: 53 ms, TR: 3000 ms, acquisition matrix: 160×95 voxels, FOV: 230 mm, NSA: 2, flip angle 90°) was performed in at least two perpendicular planes resulting in an in-plane resolution of 0.62-1.0 mm (slice thickness 4.0 mm). Routine fetal head sequences T2-weighted single-shot fast spin-echo (SSFSE) and steady-state free precession (SSFP) sequences were also performed (Supplementary Table 1). Specific absorption rate levels did not exceed 2.0 W per kilogram of body weight.

MRI Image Analysis

The retrospective classification of intracranial ICH was conducted independently by two experienced fetal neuroradiologists (D.P. and H.S., with 35 and 6 years of experience in fetal imaging respectively), based on the following characteristics: low signal intensity on EPI-T2* weighted blood-sensitive sequence in at least two perpendicular planes (Figure 2) or plus hypointensity (compared to adjacent parenchyma) on T2-TSE sequence. To distinguish hemorrhage from congested veins, a discontinuous signal loss and an asymmetric pattern can serve as differentiating factors (Figure 2, Supplementary Figures 1-3). The presence of hemorrhage, congested veins (in comparison to the control group), and related conditions including subependymal heterotopia, hydrocephalus (in cases of CM II where hydrocephalus is present, it's noteworthy that side ventricle sizes are often within 10mm, hydrocephalus in this context is defined as the third ventricle width $\geqslant$4mm[14]), and brain vasogenic edema were recorded. Venous sinus stenosis was evaluated using age-matched normal brain fetuses from the existing database[15] as a comparison (Supplementary Figure 7). The readers were blinded to the fetal MRI findings and postnatal outcomes. Disagreements were resolved by consensus. Interrater variability analysis was performed.

Vasogenic edema was defined as parenchymal hyperintensity compared with age-matched normal cases on T2-weighted sequences[16], blurring of lamination, and depleted outer CSF spaces - dry brain (Figures 2-3, Supplementary Figures 2-3).

Morphometric Measurements (inner/outer CSF spaces, posterior fossa, venous structure)

A systematic analysis of CM II and spinal defect characteristics was conducted [17] and compared between CM II with and without ICH cases. We selected 1:1 age-matched (+/-5 gestational days) fetuses from CM II with and without ICH cases, as well as AS with and without ICH cases for relevant anatomical measurements, including outer CSF spaces, maximum atrium width, third ventricle width, maximum diameter of the posterior fossa, and clivus-supraocciput angle[2], which was performed by a single radiologist (H.S.) (Supplementary Figure 4). These measurements were repeated and averaged for statistical analysis in the respective age-matched groups (CM II+ICH, CM II-ICH, AS+ICH, and AS-ICH). Morphometric measurements were rerated regarding intrarater variability analysis after 2 months. Additionally, cross-sectional areas of both the jugular vein (at the level of the atlantoaxial joint, SSFP sequence) [18] and the superior sagittal sinus (average measurements from three slices above the torcular level, T2-SSFSE sequence)[19] were assessed.

Statistics analysis

Statistical analysis was carried out using SPSS Statistics for Windows, v. 25 (IBM Corp., Armonk, NY, USA). Quantitative variables were compared using Student's t-test for independent samples, corrected for gestational age; qualitative variables were compared using Pearson's $\chi 2$.

ANOVA with post hoc Bonferroni testing was employed for morphometric measurements, effect sizes were calculated. Cohen's kappa assessed interrater agreement. Regression analysis was used to examine the association between dependent variables. Principal Component Analysis (PCA) was used for multivariate analysis and data visualization. Statistical analysis was performed by a statistical analyst with significant statistical expertise (M.W.)

Co-occurrence network of CM II with ICH

To visualize the phenotypic network associated with CM II with ICH and to distinguish it from AS with ICH, we conducted a co-occurrence analysis through Matlab R2021b19 using the data sauce of 29 CM II+ICH cases and replicated the process in the 17 AS+ICH cases. The co-occurrence matrix was constructed by extracting co-occurrence patterns from fetal MRI diagnostic features, as documented by co-authors D.P. and G.K., each possessing 35 and 16 years of experience in fetal imaging, respectively. Additionally, morphometric measurements mentioned earlier were also incorporated into the matrix. This analysis specifically focused on identifying co-occurrence patterns of "ICH" with other comorbidity features within each case. Subsequently, this dataset was utilized to create an ICH feature-centric co-occurrence network graph using Gephi software (https://gephi.org). In this network, image features served as nodes, and edges represented their co-morbidity, weighted by the frequency of co-occurrence, as derived from the previously imported matrix.

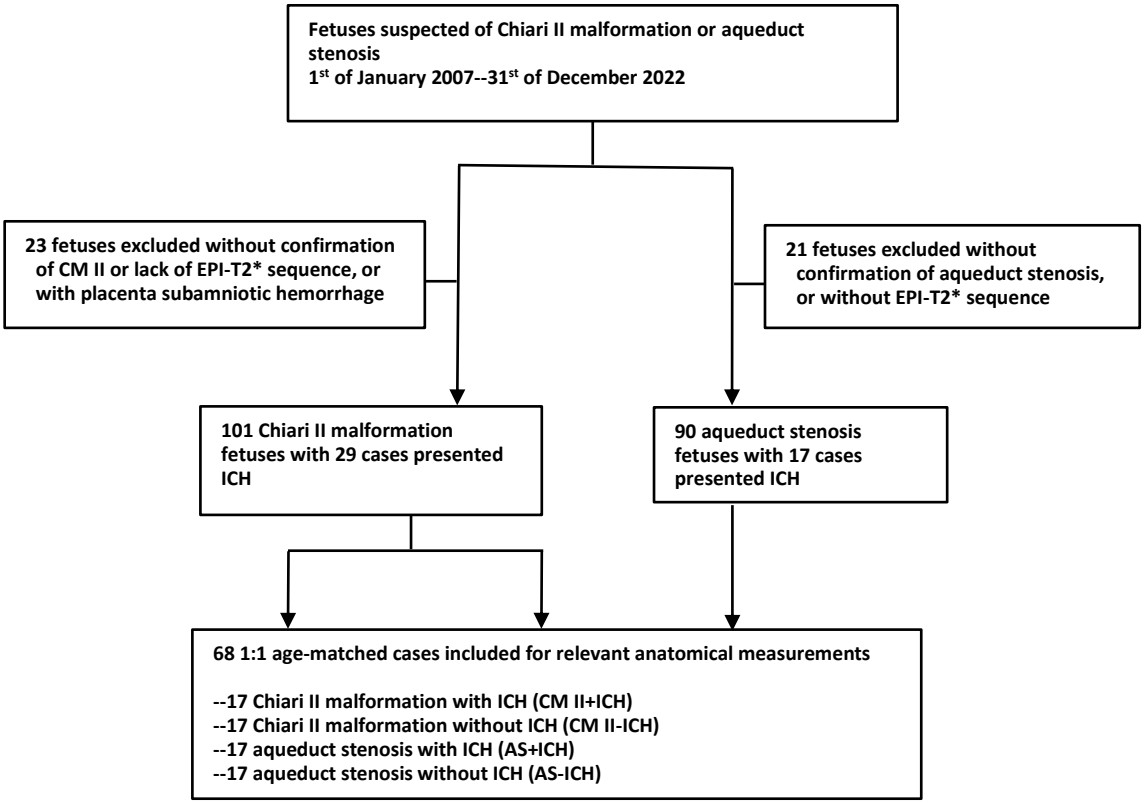

FIG 1. Flowchart of included fetuses with Chiari II malformation and aqueduct stenosis

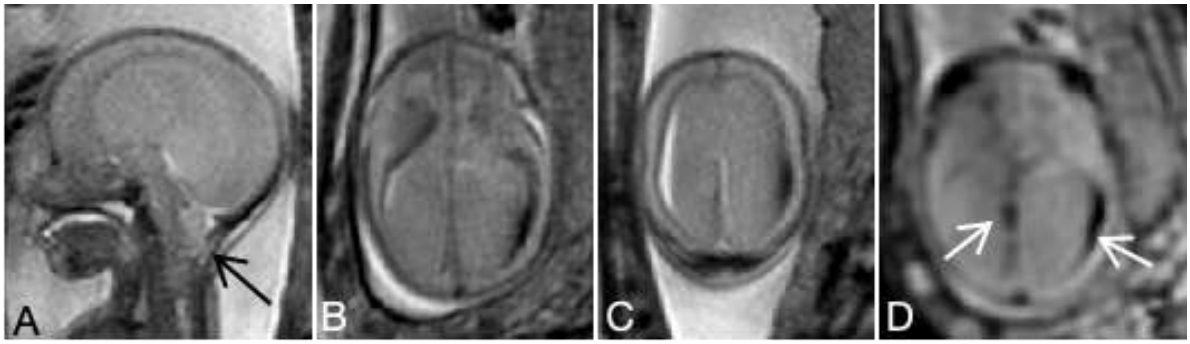

FIG 2. Prenatal MRI of a fetus with Chiari II malformation and intracranial hemorrhage (ICH). A-D: Chiari II malformation with ICH case at GW20+6. A: T2W-FSE images show the narrowing posterior cranial fossa, accompanied by a protrusion sign of the atlantooccipital membrane (black arrow). Brain parenchyma hyperintensity indicates edematous changes, with the disappearance of lamination. The outer CSF spaces appear depleted. Intraventricularly observable levels of bloody fluid with

varying degrees of sedimentation on both sides, concomitant with markedly dilated lateral ventricles, as illustrated on both T2-SSFSE and EPI-T2* blood-sensitive sequences.

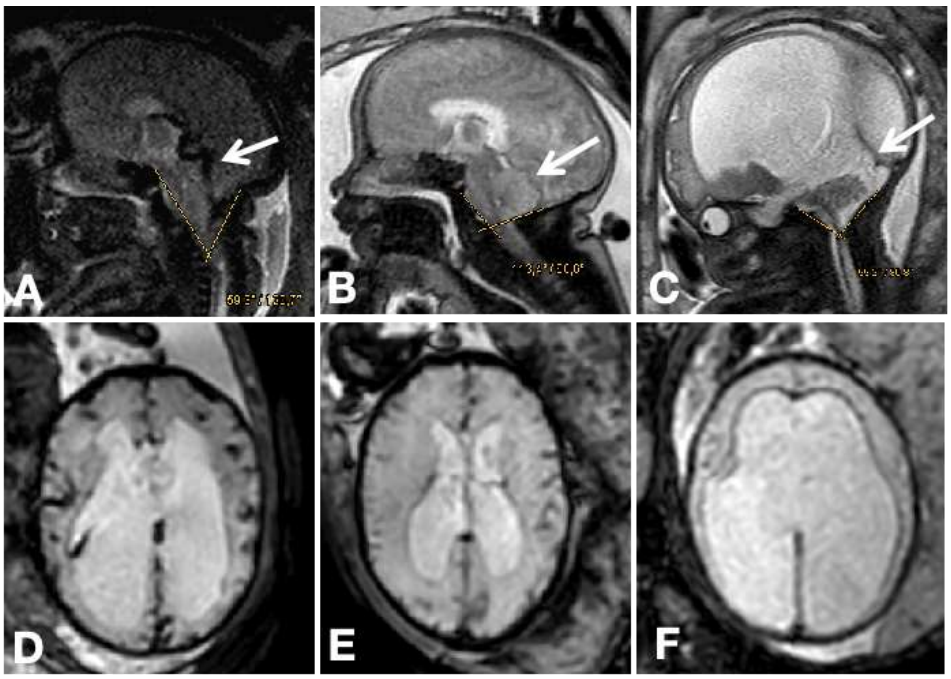

FIG 3. Comparison of clivus-supraocciput angle and venous changes among age-matched fetuses with Chiari II malformation with and without intracranial hemorrhage (ICH), and a fetus with aqueduct stenosis and ICH. A, D: Prenatal MRI scans of a fetus diagnosed with Chiari II malformation and ICH at GA35 weeks reveal congestion in the straight sinus(arrow) and cortical veins. A sharper clivus-supraocciput angle is depicted in (A). B, E: Remarkably, the same imaging modalities in a Chiari II fetus without ICH (at GA35+3 weeks) show a larger clivus-supraocciput angle without congestion in the straight sinus(arrow) and cortical veins, as seen in the ICH case. C, F: Prenatal MRI of a fetus with aqueduct stenosis and ICH performed at GA33 weeks depicts normal conditions of the straight sinus(arrow) and cortical veins. Noteworthy are the more rounded posterior horns compared to the distinct pointed posterior horns in the above two CM II cases.

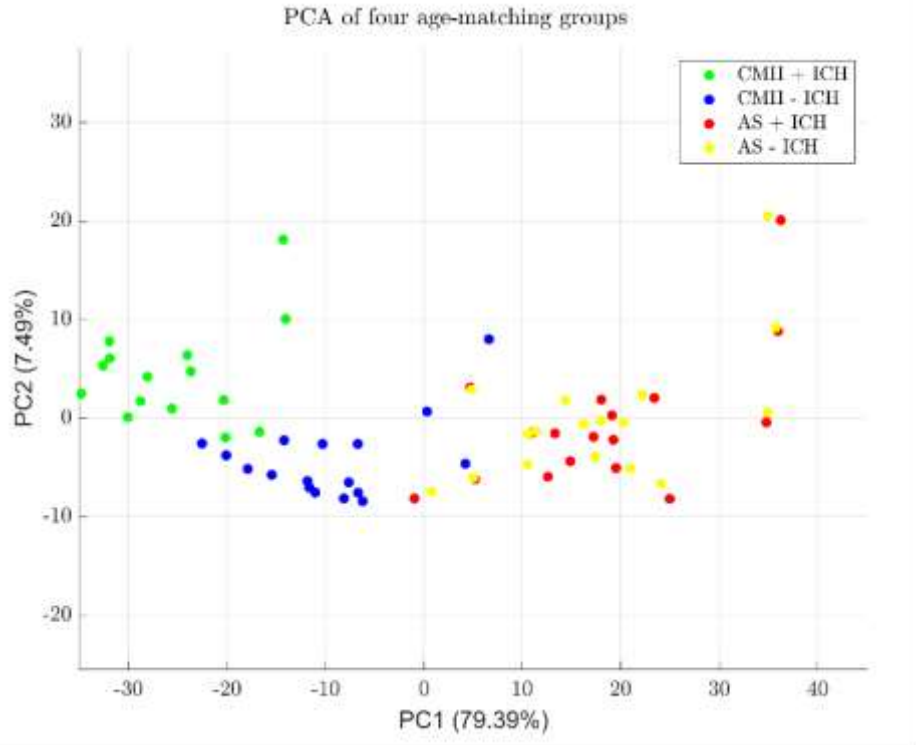

FIG 4. Principal component analysis (PCA) showed separate three clustering of these age-matched groups: group 1:CM II +ICH, group 2:CM II -ICH, group 3:AS+ICH, group 4: AS-ICH, notably AS+ICH and AS-ICH groups can't be separated. components=7.

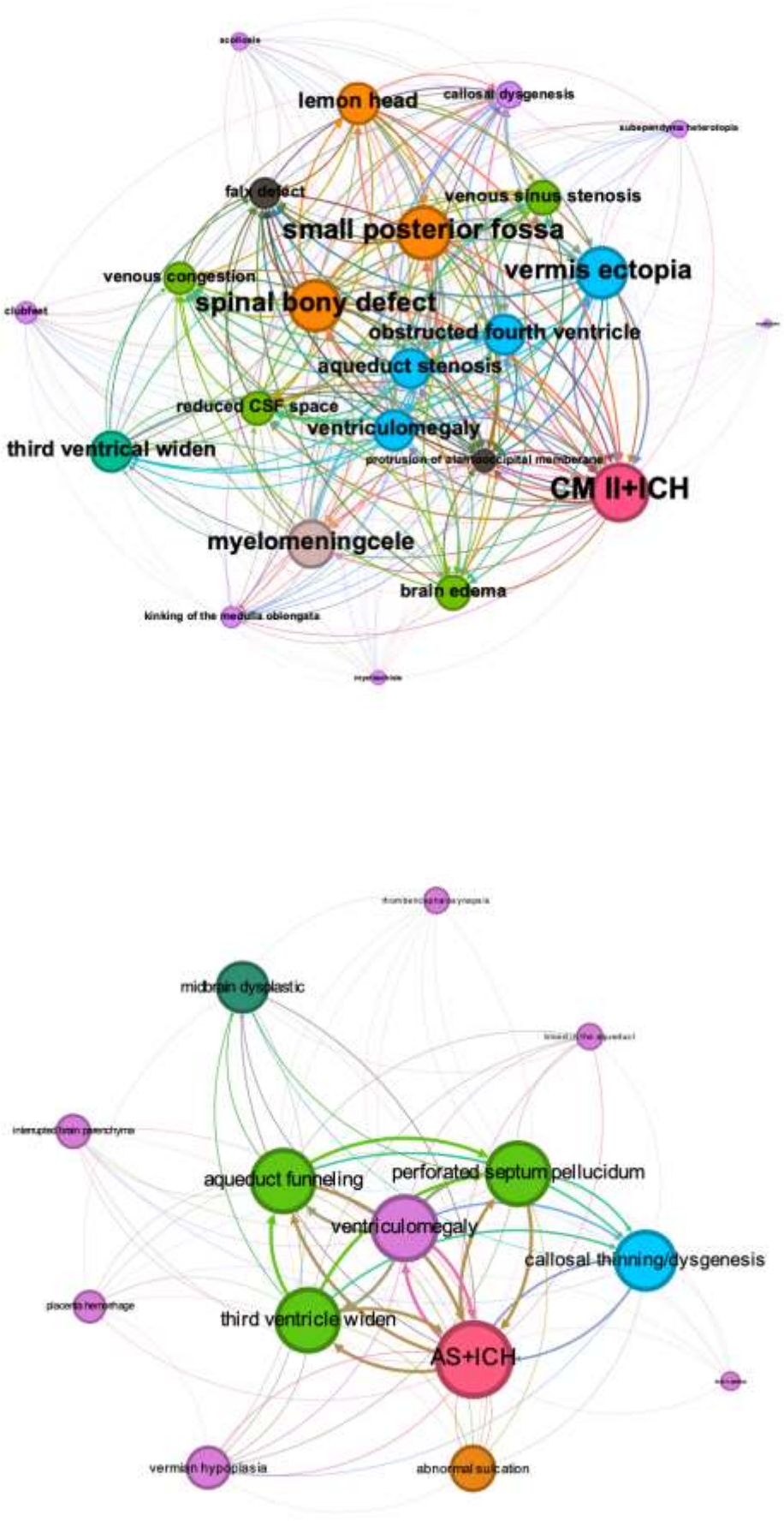

FIG 5. Comparison of co-occurrence network among fetal MRI features of Chiari II malformation (CM II) with intracranial

hemorrhage (ICH), and aqueduct stenosis (AS) with ICH. The CM II network displays a higher level of complexity, involving interactions between spinal, skull, and brain anatomical structures, while the AS network is primarily influenced by CSF blockage. We used "Betweenness Centrality" to determine node colors, where larger nodes indicate more connections, representing a higher degree of co-occurrence with other features. The weight of each edge corresponds visually to the thickness of the connecting lines and represents the pairwise frequency of co-occurrence.

RESULTS

Fetal Characteristics and Outcomes

A total of 101 fetuses with CM II and 90 controls with AS at a median gestational age of 24.4 weeks and 22.8 weeks (P=0.138) were included (Figure 1, Table 1). Prenatal diagnoses of CM II and AS were confirmed through postnatal or postmortem imaging, or autopsy, and follow-up ranged from five days to 16 years. Forty-nine fetuses in the AS group have postnatal correlations, 11/49 with hemorrhage in the cerebral aqueduct, 13/49 with rhombencephalon synapsis, 8/49 with cerebellar dysplasia, 13/49 confirmed X-linked aqueduct stenosis (L1CAM /MASA syndrome), 4/49 with unknown genesis.

The prevalence of ICH was higher in all gestational ages (summarized in Table 1) compared to AS controls (P=0.023). The incidence of ICH was slightly but not significantly higher in older (>26 weeks) fetuses (P= .213) upon comparison between CM II with and without ICH fetuses. Agreement between raters for ICH classification was substantial (κ=0.92, P < 0.001).

The 47/101 CM II cases (54/101 abortions) received in-utero (5/47) or postnatal repair surgery (42/47). In the CM II+ ICH group, 17 of 18 cases received CSF shunting, one case also underwent expansion of the posterior cranial fossa surgery. And two cases developed epilepsy. Five cases in the CM II+ ICH group had a motor functional level worse than anatomically expected.

Forty-seven cases underwent postnatal MRI (Supplementary Figures 2,3,5,6). Prenatally suspected heterotopia was confirmed via postnatal MRI (Supplementary Figure 5). And 15/47(32%) exhibited postnatal ICH (12 of them had prenatal ICH), with 6/15 presenting postnatal brain hemorrhagic infarctions, resulting in subsequent tissue loss. One case in the CM II+ ICH group developed transverse sinus thrombosis (Supplementary Figure 2). Three cases with transverse sinus stenosis exhibited abnormal drainage patterns of the superior sagittal sinus, one case developed venous malformation. Seven children still presented transverse sinus stenosis after shunting (Supplementary Figure 6).

Eleven CM II cases underwent postmortem MRI. Transverse sinus stenosis and congestion in the deep ventricular veins and medullary veins in CM II+ICH cases were identified compared to the CM II-ICH and AS cases in postmortem T2WI and SWI sequences (Supplementary Figure 7).

MRI Image Analysis

Distinct features of ICH

The location of most ICH in CM II and AS cases is along the ependyma in dotted/regional patterns, with some affecting the periventricular zone or presenting blood-fluid levels in the ventricles, notably, eight cases in the CM II group also affected the plexus, accompanied by adjacent congested veins (Figure 3, Table 2 and Supplementary Figures 2-3). ICH was all detected by EPI-T2* blood-sensitive sequences, with three cases also showing up on T2-SSFSE or T1WI sequences. In 15 out of 29 (52%) CM II + ICH cases presented dilatation (compared to the normal age-matched fetuses) of the subependymal veins (3/13, 23%), plexus veins (5/13, 38%), internal cerebral vein (4/13, 30%), superficial cortical veins (3/13 23%, mostly affected in older fetuses older than 25 gestational weeks), straight sinus (3/13, 23%) via EPI-T2* sequence, which may point to congestion present in the subsequent postnatal or postmortem SWI sequence (Figures 2-3 and Supplementary Figures 2,3,7). On the other hand, 18/29 (62%) CM II-ICH cases manifested transverse sinus stenosis (Supplementary Figure 8), and 27/29 (93%) cases were accompanied by superior sagittal sinus stenosis (Supplementary Figures 2 and 3).

Systematic analysis of CM II and spinal defect characteristics

Using all CM II cases, we found significant differences between fetuses with and without ICH in caudal extend of vermis ectopia (13.7± 0.61 versus 7.8±0.46, P<0.001), protrusion of atlantooccipital membrane (93% versus 51%, P<0.001), the incidence of hydrocephalus (90% versus 60%, P=0.003), subependymal heterotopia (31% versus 12%, P=0.028), white matter edema (86% versus 39%, P<0.001), as summarized in Table 1. Fetuses with ICH showed a slight but insignificant increase in spinal defect size (28.0±3.6 versus 21.0±1.85 mm^2, P = 0.059). Otherwise, no other significant differences were detected between the two groups.

Repeated measures ANOVA using age-matched groups' morphometric measurements

Using age-matched groups: CM II + ICH, CM II- ICH, AS + ICH, and AS - ICH, Table 2 revealed significant differences among all groups in external CSF spaces, clivus-supraocciput angle, maximum atrium width (P < 0.001), and third ventricle width (P = 0.005), the AS groups (with and without ICH) exhibited the largest size of both the atrium and third ventricle width. However, the post hoc test did not show statistically significant differences between AS + ICH and AS - ICH for all measurements. The intrarater agreement of the measurements yielded κ values ranging from 0.88 to 0.94, P < 0.001. The clivus-supraocciput angle exhibited the most significant effect size regarding ICH (Cohen's d = -2.049, Hedges correction = -1.951). Regression analysis revealed a positive correlation between the cross-sectional areas of the superior sagittal sinus and outer CSF spaces (Supplementary Figure 9).

Principal component analysis (PCA) showed three separate clustering of these four age-matched groups (Figure 4), the components=7. Notably, the AS+ ICH and AS- ICH groups were not distinguishable.

Co-occurrence network of ICH

The co-occurrence networks of MRI diagnostic features in both CM II+ICH and AS+ ICH cases were visualized using Gephi software (Figure 5). While the AS network is primarily influenced by aqueduct blockage, in the more complex network of CM II, except spinal

bony defect, small posterior fossa, and vermis ectopia emerge as core features[20] demonstrating the largest size of nodes with thickest connections, indicating their strong co-occurrence, there are more contributing features involved including reduced outer CSF spaces, the protrusion sign of the atlantooccipital membrane, venous congestion, and venous sinus stenosis.

DISCUSSION

In this study, in line with the findings of Didier et al.[6], we identified ICH in 29 /101(29%) CM II cases using the EPI-T2* blood-sensitive sequence, indicating a higher prevalence compared to the AS group (17/90, 19%, P=0.023). While the AS+ICH group exhibited the most severe degree of hydrocephalus, the higher incidence of ICH in the CM II group suggests additional contributing factors beyond obstructive CSF dynamics and extreme stretching and thinning of the ventricular wall, which can lead to the impairment of the immature ependyma[21, 22]. Hemorrhages predominantly occurred at the ependyma in both groups, notably, eight cases in the CM II group also affected the plexus, accompanied by adjacent congested veins (Figure 3, Supplementary Figures 2-3). The presence of dilated veins and sinus stenosis (Supplementary Figures 2,3,6) suggests the potential role of venous congestion in the CM II group in ICH etiology. The incidence of ICH was slightly but not significantly higher in older (>26 weeks) CM II fetuses (P= 0.213), which could be due to the deeper extent of vermis ectopia accompanied by increased ventriculomegaly[6], and vanishing outer CSF spaces tend to develop in later gestation (bias may exist considering a small sample size in older fetuses). Moreover, anatomical measurements highlight the significance of the sharper clivus-supraocciput angle, which exhibited a substantial effect size concerning ICH in CM II. The co-occurrence network visualizes a more intricate interplay of contributing factors in CM II.

Deeper extend of vermis ectopia, a significantly higher frequency of hydrocephalus and subependymal heterotopia as well as brain vasogenic edema, and a more frequent occurrence of the protrusion sign of the atlantooccipital membrane were found in the CM II+ICH group. The elongation and kinking of the medulla oblongata in CM II, along with increased intraventricular pressure—partly due to associated aqueductal stenosis—may result in brainstem compression and partial obstruction of venous return, leading to tissue edema. The proliferation of the capillary network in developing brain tissue can also be impaired, leading to both ischemic and hemorrhagic microinfarcts (Supplementary Figures 2-3). Damaged ependyma may fail to regulate the transport of fluid, ions, and small molecules between cerebral parenchyma and ventricular fluid, contributing to the higher incidence of hydrocephalus in the ICH group [23, 24].The posterior and downward protrusion of the vermis creates a concavity in the atlantooccipital membrane, resembling a notch just below the level of the torcula (Supplementary Figure 10), where the transverse sinus is situated. This explains the occurrence of transverse sinus stenosis in certain cases (Supplementary Figures 6 and 8).

On the other hand, the cross-sectional areas of the jugular vein did not exhibit significant variation among the groups, suggesting that venous drainage blockage likely occurs at the cranial cervical junction. These findings(evidence of blockage affecting inner and outer CSF outflow as well as venous drainage) collectively indicate the potential existence of a complex feedback loop in CM II cases [5]. As illustrated by the “co-occurrence network”, this cycle is characterized by a hypoplastic posterior cranial fossa and cerebellar prolapse that generates abnormal tension within the constrained bone container. Consequently, this tension leads to the compression of crucial structures such as the transverse sinus and superior sagittal sinus, which are attached to the crista galli at the interhemispheric space just beneath the cranial vault [8, 25] with the side walls lacking muscle structure could be compressed by the expanding and swollen parenchyma, resulting in vasogenic edema. Simultaneously, anatomical venous sinus obstruction can further elevate venous outflow resistance[26, 27], resulting in increased venous pressure that may contribute to hemorrhage and the development of communicant-type hydrocephalus. This is compounded by defective CSF absorption due to increased venous pressure, with the elevated venous pressure itself primarily resulting from the constriction of the posterior cranial fossa structures [3]. Although vermis ectopia is not a true herniation because intracranial hypertension is not the primary mechanical force causing this displacement[1], venous congestion and subsequent edema may exacerbate the vermis ectopia(Supplementary Figure 11).

Both mechanisms are known to hinder venous drainage leading to deep venous congestion and dilatation[3, 28], where mostly the deep paraventricular veins could be affected, as fetal microcirculation may lack full development of the cortical venous drainage[29]. More clinical morbidity and postnatal disability happened in the CM II with ICH cases, which could be attributed to more severe morphological deformation: a deeper extent of vermis ectopia and a sharper clivus-supraocciput angle, leading to more severe CSF and venous drainage blockage in the posterior fossa. In some cases, hemorrhagic infarction was suspected to occur after shunt placement, underscoring the importance of including MRV in the prenatal diagnosis of CM II with ICH to evaluate venous conditions before shunting, surgeons may need to exercise caution when adjusting the speed and pressure during CSF shunting to mitigate blood pressure fluctuations and should closely monitor the child postoperatively. Addressing this complex interplay further supports the concept of prenatal surgery, which leads to an expansion of outer CSF spaces and presumably the reestablishment of proper CSF dynamics[30, 31] and improves the venous drainage system (Supplementary Figure 12). The study's findings hold promise for clinical practice, potentially optimizing the selection of surgical intrauterine repair. In some institutions, ICH has been considered unrelated to the primary disease and excluded from surgery[10]. The study's insights into ICH prevalence and its association with CM II challenge this notion.

Our study has several limitations. Firstly, incorporating AS as a control might be controversial regarding the parenchymal, meningeal, and osseous architecture differences though it aligns with the aim of this study—to validate the common prevalence of ICH and contributing factors in CM II comparing another cohort presenting ICH and hydrocephalus. Secondly, although not significantly different, the younger GA of the AS fetuses might potentially influence the observed prevalence of ICH in this study. Thirdly, different field strengths led to different parameters for the GRE sequence, the potential for interval hemorrhage, and unavoidable differences in the timing of imaging could have influenced the prevalence of ICH between groups. Fourthly, our comparably large cohorts of CM II and AS were collected over a relatively large time span without having undergone in-utero repair. This is advantageous, as this cohort may serve as “historic” controls with high imaging quality, however disadvantageous as it does not allow for any conclusion on the impact of fetal

surgery on the course of IVH in CM II. We are convinced that the examined phenomenon and imaging features allow for interesting comparative and outcome studies in cohorts treated surgically.

Table 1: Fetal demographics and MRI characteristics.

Characteristics	Fetuses with Chiari II malformation(n=101)	Fetuses with aqueduct stenosis(n=90)	P*
Male fetuses (%)	47/101 (46.5)	42/90(46.7)	0.669
Median gestational age at fetal MRI (weeks)	24.4(16.7-37.3)	22.8 (17.1-41)	0.138
Timing of MRI			
≤26 weeks	70	66	
>26 weeks	31	24	
Incidence of ICH			
All gestational ages (%)	29/101 (28.7)	17/90 (18.9)	0.023
≤26 weeks (%)	20/71(28.1)	14/64 (21.8)	0.044
>26 weeks (%)	9/30(30)	3/26 (11.5)	0.016

Table 2: Systematic analysis of Chiari II and spinal defect characteristics and comparisons between with and without ICH cases.

Parameters	CM II with ICH (n=29)	CM II without ICH (n=72)	P*
Male fetuses (%)	45(13/29)	48(35/72)	0.730
Median gestational age at fetal MRI (weeks)	25.7(16.7-35.9)	24.1(18-37.3)	0.338
Incidenceof hydrocephalus (%)	90(26/29)	60(43/72)	0.003
Incidence of brain edema (%)	86(25/29)	39(28/72)	<0.001
Incidence of heterotopia (%)	31(9/29)	12(9/72)	0.028
Anatomic level (%)			
Sacral	45(13/29)	38(27/72)	0.496
Lumbar	31(9/29)	50(36/72)	0.083
Thoracic	24(7/29)	12(9/72)	0.251
Size of defect(mm)	28.0 a±1.95	21.0 a±1.49	0.059
Vermian displacement (%)			
C1-C3	45(13/29)	56(40/72)	0.329
C4-C7	55(16/29)	44(32/72)	0.329
Depth of vermis downward displacement(mm)	13.7 a±0.61	7.8 a±0.46	<0.001
Protrusion sign of atlantooccipital memberane (%)	93 (27/29)	51(37/72)	<0.001

Data are given as median (range), n (%) or mean ± SD. *Comparison between with and without ICH cases: quantitative variables compared using Student's t-test for independent samples; qualitative variables compared using Pearson's x2
a Estimated means based on an average GA of: GA = 24.3.

Table 3: Morphometric measurements comparisons among Chiari II with and without ICH and aqueduct stenosis with ICH groups.

Value	CM II + ICH(n=17) Mean	SD	CM II - ICH(n=17) Mean	SD	AS + ICH(n=17) Mean	SD	AS - ICH(n=17) Mean	SD	P*
External CSF spaces	10.7	4.2	16.8	6.8	33.8	6.0	32.9	5.3	<0.001
Maximum Atrium width(mm)	18.6	5.2	12.4	3.8	23.2	5.2	24.3	5.5	<0.001
third ventricle width(mm)	5.7	2.0	3.9	3.0	6.9	2.8	6.2	2.6	0.005
Max.diameter of the posterior fossa (mm)	22.2	4.5	22.2	4.4	30.4	7.1	30.6	6.9	<0.001
clivus-supraocciput angle(degree)	54.3	8.7	73.2	7.3	90.7	7.9	89.7	8.1	<0.001
cross-section area of jugular vein (mm2)	6.8	2.2	6.8	2.4	5.9	1.2	6.2	1.2	0.322
cross-section area of superior sagittal sinus(mm2)	3.9	1.7	5.1	2.7	13.2	6.6	12.4	6.5	<0.001

SD = standard deviations, measurement of the cross-section area of the jugular vein was averaged left and right sides.

CONCLUSIONS

ICH is intricately linked to CM II in the fetal stage, with a complex interplay of factors contributing to a vicious cycle of venous congestion and altered CSF dynamics. Pathophysiological alterations of ICH underlie a more severe phenotype of CM II, which should be considered a candidate for in-utero surgery.

ACKNOWLEDGMENTS

The authors would like to thank Professor Harvey. B. Sarnat for the comment on the potential etiology of intracranial hemorrhage in CM II, as well as the radiographers of the Division of Neuro- and Musculoskeletal Radiology at the Medical University of Vienna for their enthusiastic support.

REFERENCES

1. Sarnat HB. Disorders of segmentation of the neural tube: Chiari malformations. *Handb Clin Neurol* 2008;87:89-103
2. Woitek R, Dvorak A, Weber M, et al. MR-based morphometry of the posterior fossa in fetuses with neural tube defects of the spine. *PLoS One* 2014;9:e112585
3. Tamburrini G, Frassanito P, Iakovaki K, et al. Myelomeningocele: the management of the associated hydrocephalus. *Childs Nerv Syst* 2013;29:1569-1579
4. McLone DG, Dias MS. The Chiari II malformation: cause and impact. *Childs Nerv Syst* 2003;19:540-550
5. Fukuoka T, Nishimura Y, Hara M, et al. Chiari Type 1 Malformation-induced Intracranial Hypertension with Diffuse Brain Edema Treated with Foramen Magnum Decompression: A Case Report. *NMC Case Rep J* 2017;4:115-120
6. Didier RA, Martin-Saavedra JS, Oliver ER, et al. Fetal Intraventricular Hemorrhage in Open Neural Tube Defects: Prenatal Imaging Evaluation and Perinatal Outcomes. *AJNR Am J Neuroradiol* 2020;41:1923-1929
7. Zamlynski J, Olejek A, Koszutski T, et al. Comparison of prenatal and postnatal treatments of spina bifida in Poland--a non-randomized, single-center study. *J Matern Fetal Neonatal Med* 2014;27:1409-1417
8. Cinalli G, Russo C, Vitulli F, et al. Changes in venous drainage after posterior cranial vault distraction and foramen magnum decompression in syndromic craniosynostosis. *J Neurosurg Pediatr* 2022:1-12
9. Lauzier DC, Chiang SN, Chatterjee AR, et al. Idiopathic Intracranial Hypertension and Vascular Anomalies in Chiari I Malformation. *Neurosurg Clin N Am* 2023;34:175-183
10. Putbrese B, Kennedy A. Findings and differential diagnosis of fetal intracranial haemorrhage and fetal ischaemic brain injury: what is the role of fetal MRI? *Br J Radiol* 2017;90:20160253
11. Heaphy-Henault KJ, Guimaraes CV, Mehollin-Ray AR, et al. Congenital Aqueductal Stenosis: Findings at Fetal MRI That Accurately Predict a Postnatal Diagnosis. *AJNR Am J Neuroradiol* 2018;39:942-948
12. Barkovich AJ, Newton TH. MR of aqueductal stenosis: evidence of a broad spectrum of tectal distortion. *AJNR Am J Neuroradiol* 1989;10:471-476
13. Prayer D, Malinger G, De Catte L, et al. ISUOG Practice Guidelines (updated): performance of fetal magnetic resonance imaging. *Ultrasound Obstet Gynecol* 2023;61:278-287
14. Garel C. *MRI of the Fetal Brain: Normal Development and Cerebral Pathologies.* Stuttgart, Germany: Springer; 2004.
15. Stuempflen M, Taymourtash A, Kienast P, et al. Ganglionic eminence: volumetric assessment of transient brain structure utilizing fetal magnetic resonance imaging. Ultrasound Obstet Gynecol. 2023;62(3):405-413. doi: 10.1002/uog.26232.
16. Shi H, Prayer F, Kienast P, et al. Multiparametric prenatal imaging characterization of fetal brain edema in Chiari II malformation might help to select candidates for fetal surgery. *in press in Eur Radiol.* 2024; https://doi.org/10.1007/s00330-024-10729-0
17. Avesani G, Perazzolo A, Elia L, et al. Fetal MRI prior to intrauterine surgery of open neural tube defects: What does the radiologist need to know. *Radiol Med* 2022
18. Fu SJ, Xu JB, Liu X, et al. Quantitative Evaluation of a Cross-Sectional Area of the Fetal Straight Sinus by Magnetic Resonance Imaging and Its Clinical Value. *Front Neurol* 2022;13:875402
19. Bateman GA, Lechner-Scott J, Bateman AR. Modelling of the dilated sagittal sinuses found in multiple sclerosis suggests increased wall stiffness may be a contributing factor. *Sci Rep* 2022;12:17575
20. Barabasi AL, Gulbahce N, Loscalzo J. Network medicine: a network-based approach to human disease. *Nat Rev Genet* 2011;12:56-68
21. Sarnat HB. Regional differentiation of the human fetal ependyma: immunocytochemical markers. *J Neuropathol Exp Neurol* 1992;51:58-75
22. Sarnat HB. Histochemistry and immunocytochemistry of the developing ependyma and choroid plexus. *Microsc Res Tech* 1998;41:14-28
23. Sarnat HB. Ependymal reactions to injury. A review. *J Neuropathol Exp Neurol* 1995;54:1-15
24. Del Bigio MR. Ependymal cells: biology and pathology. *Acta Neuropathol* 2010;119:55-73
25. Lublinsky S, Friedman A, Kesler A, et al. Automated Cross-Sectional Measurement Method of Intracranial Dural Venous Sinuses. *AJNR Am J Neuroradiol* 2016;37:468-474
26. Markey KA, Mollan SP, Jensen RH, et al. Understanding idiopathic intracranial hypertension: mechanisms, management, and future directions. *Lancet Neurol* 2016;15:78-91
27. Zhao K, Gu W, Liu C, et al. Advances in the Understanding of the Complex Role of Venous Sinus Stenosis in Idiopathic Intracranial Hypertension. *J Magn Reson Imaging* 2022;56:645-654
28. Conner ES, Foley L, Black PM. Experimental normal-pressure hydrocephalus is accompanied by increased transmantle pressure. *J Neurosurg* 1984;61:322-327
29. Okudera T, Huang YP, Fukusumi A, et al. Micro-angiographical studies of the medullary venous system of the cerebral hemisphere. *Neuropathology* 1999;19:93-111
30. Mufti N, Aertsen M, Ebner M, et al. Cortical spectral matching and shape and volume analysis of the fetal brain pre- and post-fetal surgery for spina bifida: a retrospective study. *Neuroradiology* 2021;63:1721-1734
31. Jakab A, Payette K, Mazzone L, et al. Emerging magnetic resonance imaging techniques in open spina bifida in utero. *Eur Radiol Exp* 2021;5:23

SUPPLEMENTAL FILES

Table 1: Acquisition parameters of T2-TSE and SSFP sequence

Sequence	FOV	matrix	Slice thickness /Gap(mm)	Reconstructed Voxel Size(mm)	TR (ms)	TE (ms)	Flip angle	NSA

T2-SSFSE	200-230	256x256	2.0-4.4	0.90/0.90/4.0	3000	100&140	90°	1
SSFP	260	192x219	6.0/-3.0	1.02/1.02/6.00			80°	1

Table 2: Location of ICH in Chiari II malformation (CM II) and aqueduct stenosis (AS) cases

Location	ependyma	blood level in the ventricle	periventricular zone	plexus	Germinal matrix
CM II (*n*=29)	27	2	2	8	2
AS (*n*=17)	15	1	0	1	1

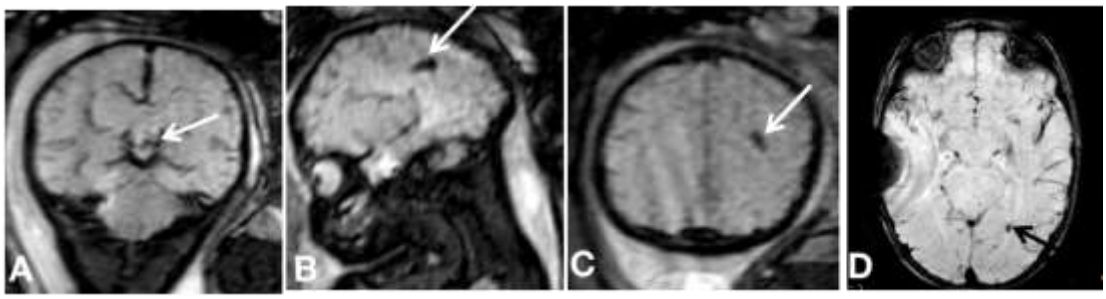

Figure 1: Examples of distinguishing hemorrhage from congested veins: the presence of a discontinuous signal loss and an asymmetric appearance can serve as differentiating factors**.**

This prenatal MRI EPI-T2* sequence depicts a CM II case conducted at GA 34+5. A: Symmetric appearance of the deep veins (arrow). B, C: Dotted shape hemorrhage (arrows) are shown on two perpendicular planes illustrating discontinuous signal loss and an asymmetric pattern, as subsequently confirmed by a follow-up postnatal MRI-SWI (arrow).

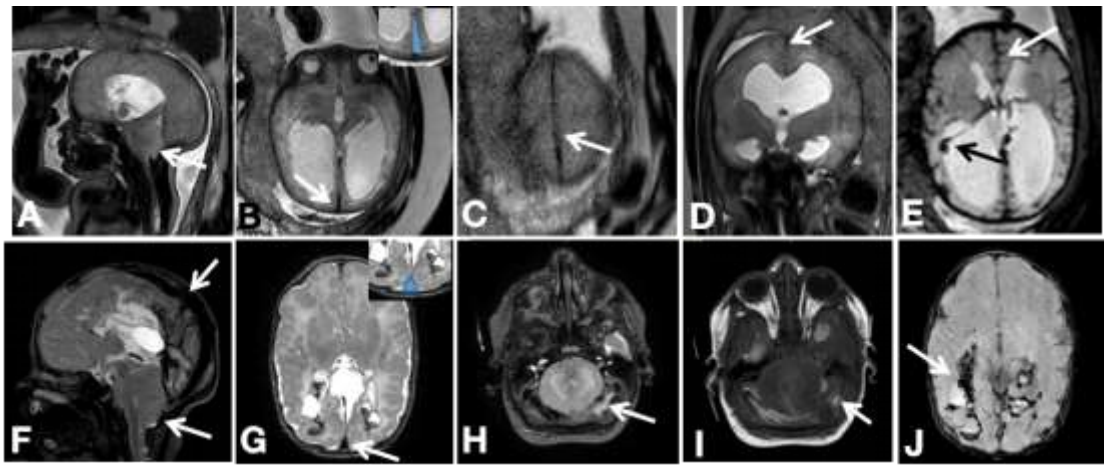

Figure 2. A fetus with Chiari II malformation and ICH developed transverse sinus thrombosis demonstrated on postnatal follow-up imaging.

A-E: Fetal MRI was performed at GA35 weeks. A: Mid-sagittal T2W-FSE image shows hypoplastic posterior cranial fossa, accompanied by vermis extending into the spinal canal up to the level of C7/C1, and protrusion sign of atlantooccipital memberane (white arrow). B-D: Edematous changes are observed in the brain parenchyma, and the superior sagittal sinus is compressed by the swollen brain parenchyma and narrowed (white arrow). E: T2-weighted blood-sensitive sequence reveals hemorrhage within the plexus and adjacent congested veins shaped like hockey (black arrow), and the congested cortical veins are also shown (white arrow). F-J: Subsequent postnatal images, obtained 14 days after birth and MMC repair surgery and EVD shunt placement. F-G: Restored CSF spaces are shown under the vermis, and superior sagittal sinus is perfused and dilated (arrows) compared to prenatal MRI. Multiple intracerebral hemorrhages are evident in both the temporal and occipital lobes (right > left). These hemorrhages encompass regions such as the calcarine sulcus and visual pathway on both sides. H-I: Transverse sinus thrombosis is shown as hyperintensity on both T2WI and T1WI. J: Notably, there are congested veins adjacent to the collapsed right occipital horn as shown on SWI sequence.

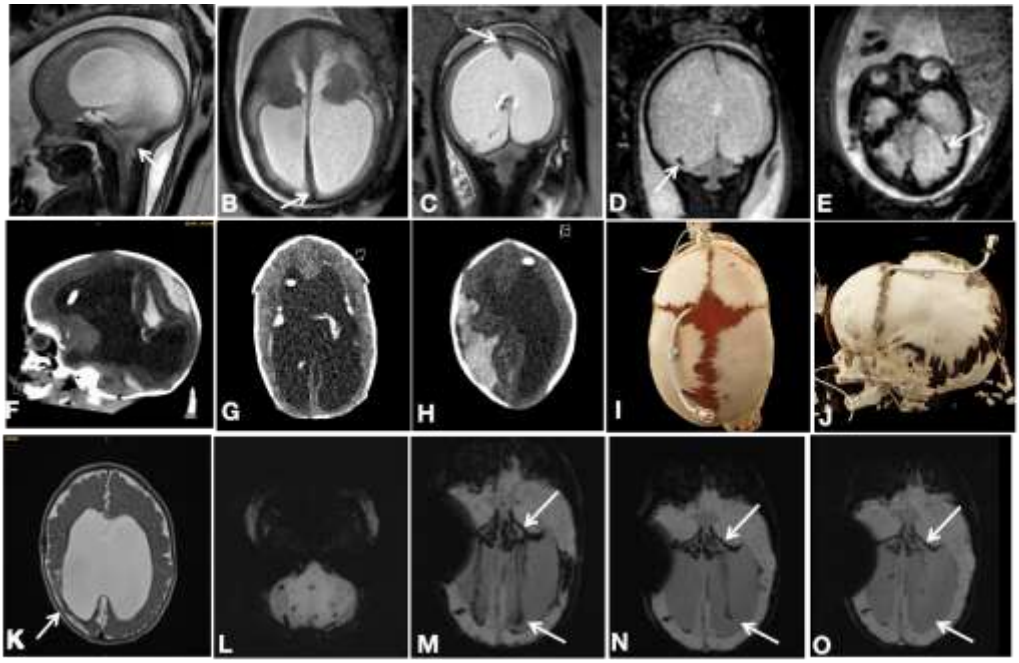

Figure 3. Fetuses with Chiari II malformation and ICH developed severe postnatal ICH after postnatal MMC repair surgery and VP shunt.

A-E: Prenatal MRI was performed at GA 32+3 weeks. A: In known Chiari II malformation, the cerebellar tonsils and the vermis protracted through the spinal canal through the foramen magnum. The pons is narrowed and the brainstem appears elongated overall. B, C: Edematous changes are observed in the brain parenchyma, and the transverse sinus and superior sagittal sinus are compressed by the swollen brain parenchyma and narrowed (white arrow). D, E: T2-weighted blood-sensitive sequence reveals hemorrhage within the plexus and ependyma, note the adjacent congested veins (arrow in E).

F-J: Postnatal CT was performed under consideration of ICH after shunt. Multiple parenchymal hemorrhages are evident accompanied by perifocal edema. Additionally, subdural blood lamella as well as subependymal and plexus hemorrhages are shown on both sides. Noting the separation of cranial sutures by the swollen and expanding brain.

K-L: ***Postnatal MRI demonstrates*** hemosiderin deposits in both the brain (with leukomalacia) and the cerebellum. M-O: ***Follow-up postnatal MRI scans obtained at three different time points (8 months, 17 months, and 22 months of age, respectively) demonstrate th***e gradual alleviation of congestion in the deep ventricular veins (white arrows).

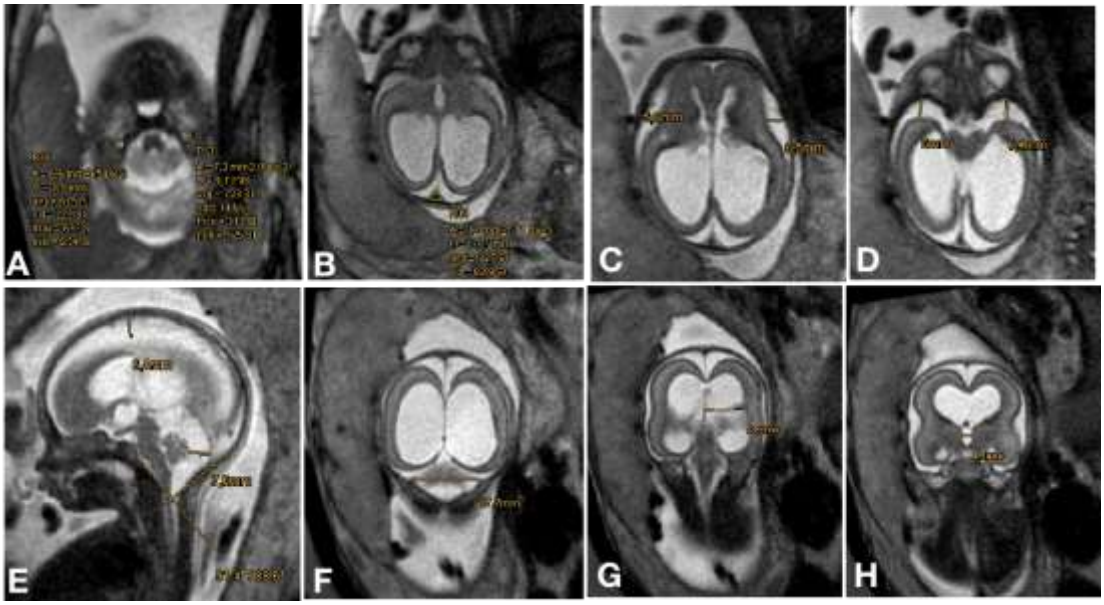

Figure 4: Example of variants measurement via PACS tools in a fetus with aqueduct stenosis at GA 23+4 weeks.

A: The cross-section area of the jugular vein was measured at the level of the atlantoaxial joint, SSFP sequence, averaged left from right.

B: Superior sagittal sinus was calculated by average 3 slices' measurements above the torcular level, delineating the flow void, T2-SSFSE sequence.

C, D, and E: Outer cerebrospinal fluid spaces are calculated by summarizing the insular cistern and temporobasal cistern (axial plane), as well as central and retrocerebellar subarachnoid spaces (mid-sagittal plane). E: The clivus-supraocciput angle was measured using two lines: The first line was placed along the postero-superior surface of the clivus, connecting the most cranial part of the clivus and the anterior border of the foramen magnum (basion). The second line was placed along the superior surface of the supraocciput, cutting the posterior border of the foramen magnum.

F: To measure the maximum diameter of the posterior fossa, distance between the medial surfaces of the lateral bony margins of the posterior fossa at the level of the lateral insertions of the tentorium cerebelli was depicted on coronal T2-weighted SSFSE or SSFP sequences.
G and H: The atrium width of the lateral ventricle and third ventricle width were measured at the coronal plane.

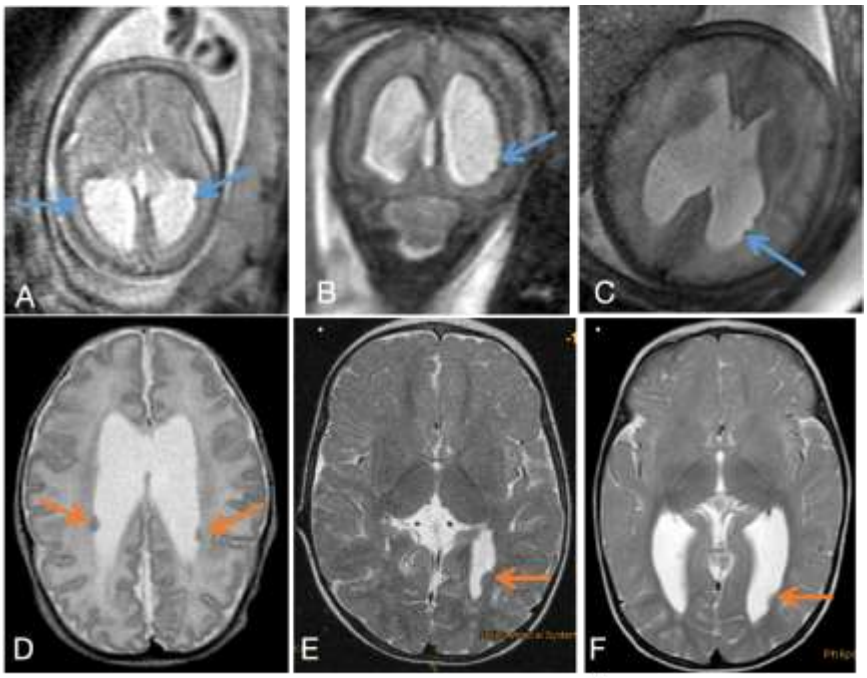

Figure 5: Prenatal and postnatal follow-up MRI of three CM II + heterotopia cases.

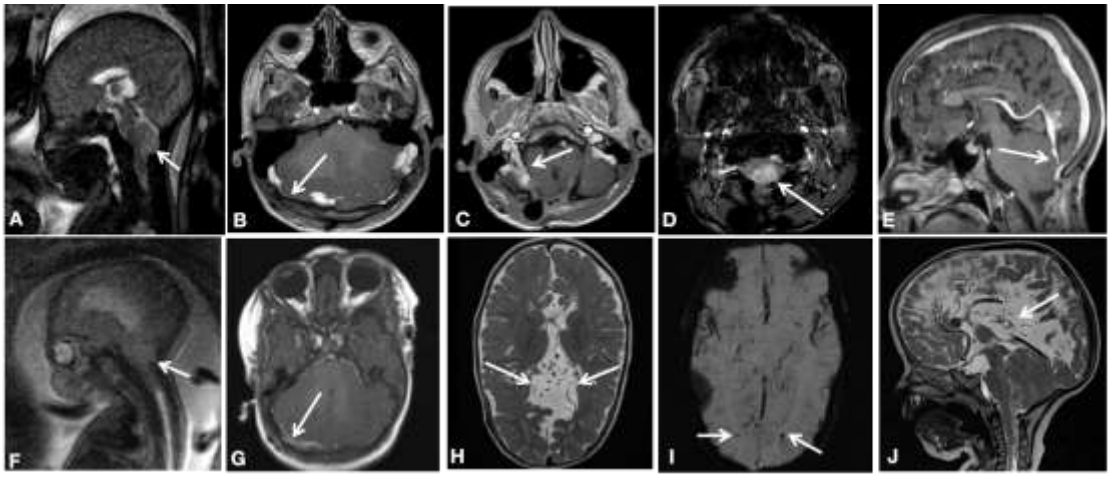

Figure 6: Postnatal MRI of two cases shows abnormal venous structure.
A-E: Fetal MRI of a CM II with ICH case showing protrusion of atlantooccipital memberane (arrow). B, C: Postnatal MRI shows transverse sinus stenosis (arrow) and abnormal drainage patterns of the superior sagittal sinus that drains into the right sigmoid sinus (white arrows). D: Microhemorrhages are visible on the SWI image (arrow). E: Sagittal contrast image demonstrates proximal straight sinus stenosis(arrow).
F-J: Prenatal MRI of a Chiari II with ICH case showing protrusion of atlantooccipital memberane (arrow). G: Postnatal MRI shows transverse sinus stenosis or dysplasia (arrow). H, J: Within the enlarged interhemispheric space, there are now accentuated vascular structures, which probably correspond to branches of the internal cerebral vein. This appears to be a long-term aplasia of the transverse sinus and left sigmoid sinus, exist (only a short section is likely to have been created, the sinus on the right side also appears rather hypoplastic). I: Microhemorrhages are visible on the SWI image (arrow).

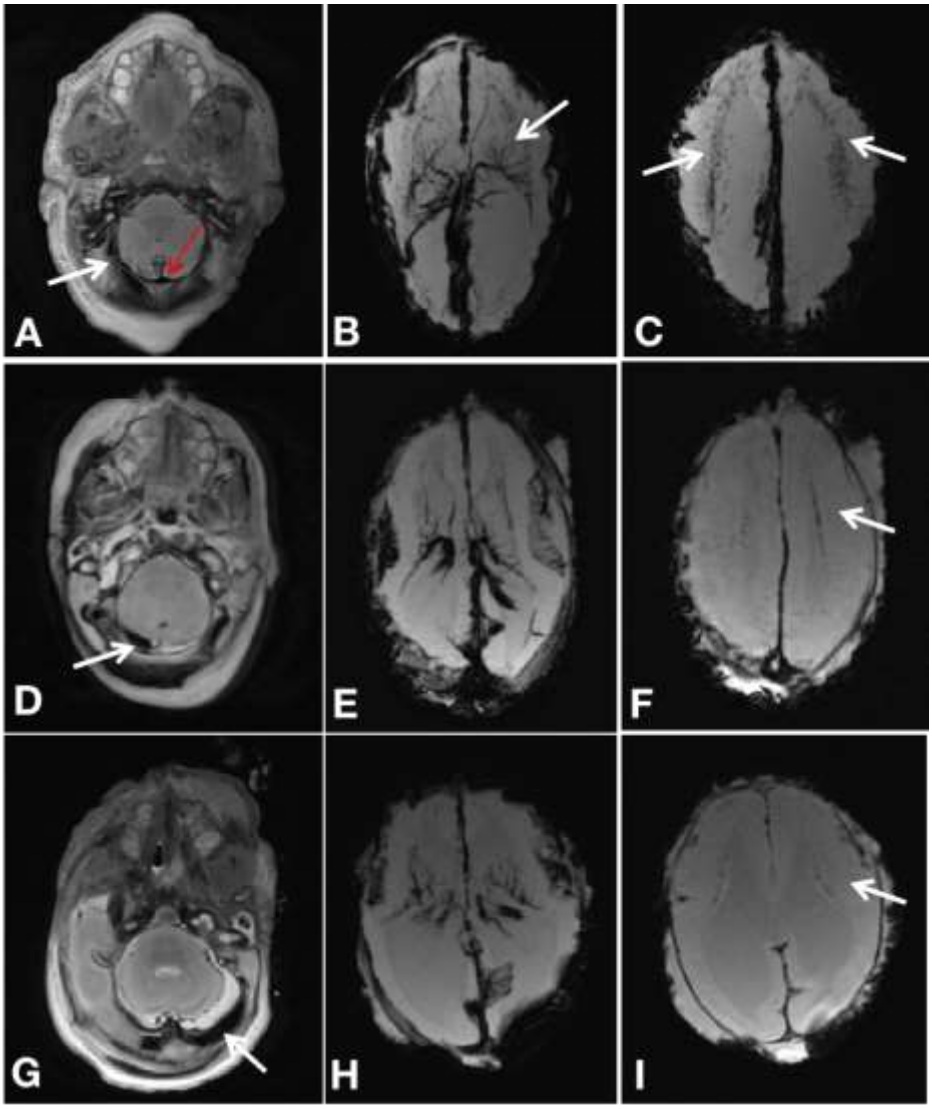

Figure 7: Postmortem MRI of three representative cases: Chiari II malformation with and without intracranial hemorrhage (ICH), and aqueduct stenosis with ICH.

A-C: Postmortem MRI of a Chiari II with ICH cases was conducted at GA22+3 weeks, noting transverse sinus stenosis (white arrow) and the congestion of vermian veins (red arrow), as well as congestion in the deep veins and medullary veins (white arrows).

D-F: Postmortem MRI of a Chiari II without ICH cases was conducted at GA21+6 weeks. T2WI sequence shows transverse sinus stenosis(arrow) but to a lesser extent compared to the above case, the SWI images does not show the deep medullary veins (white arrow) congestion change.

G-I: Postmortem MRI of an aqueduct stenosis case was performed at GA22+2 weeks, both the transverse sinus and the deep medullary veins look normal.

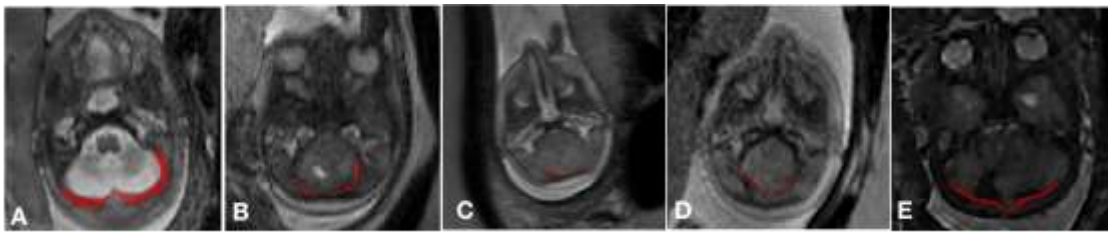

Figure 8: Segmentation of the transverse sinus in some cases using ITK-snap.

A: Segmentation of the transverse sinus in an aqueduct stenosis (AS) control case.

B-E: Segmentation of the transverse sinus (delineating the flow void) in four CM II cases illustrates stenosis as compared to the above AS control case, specifically with extreme focal compression by the cerebellum shown in E.

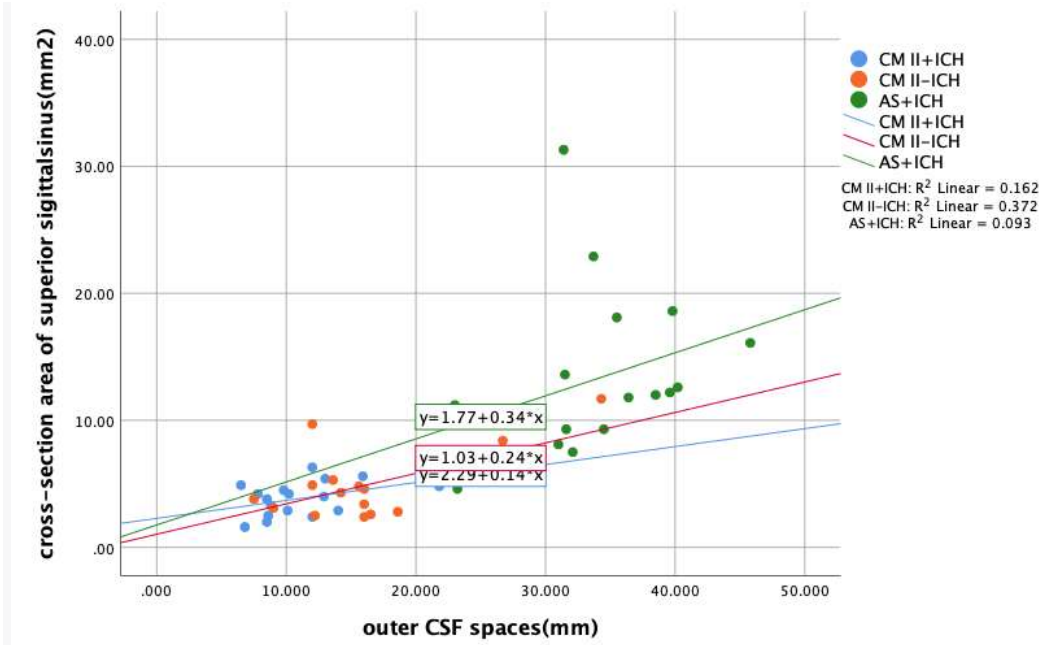

Figure 9: Scatter plots show different distributions of outer CSF spaces and cross-sectional areas of the superior sagittal sinus of the 3 age-matched groups. Regression analysis reveals a positive correlation between the cross-sectional areas of the superior sagittal sinus and outer CSF spaces.

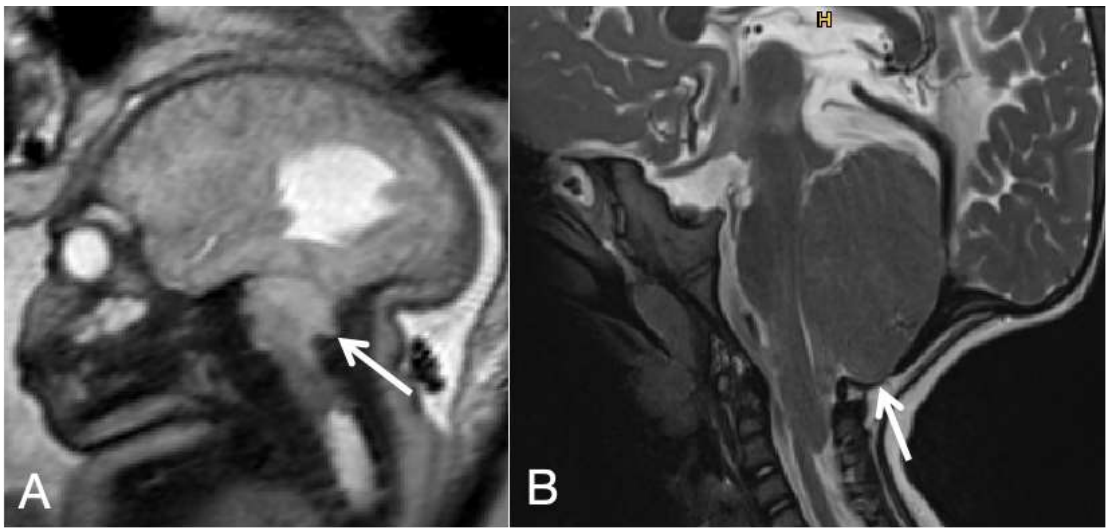

Figure 10: Protrusion of the atlantooccipital membrane showed in a fetus with Chiari II malformation.
A: The posterior and downward protrusion of the vermis (indicated by the white arrow) creates a concavity in the atlantooccipital membrane, resembling a notch just below the level of the torcula. B: This is precisely where the transverse sinus is situated as illustrated in the postnatal image.

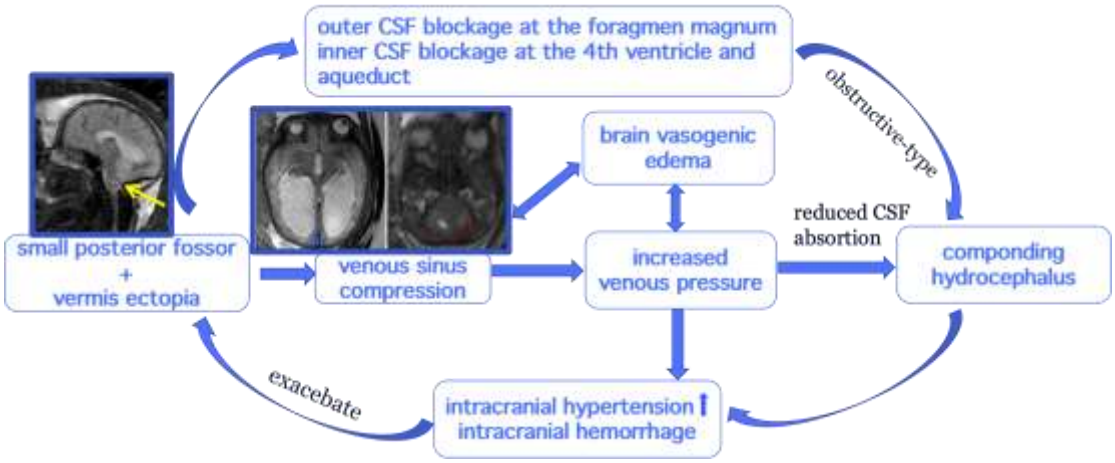

Figure 11: The hypothesized vicious cycle in Chiari II malformation accompanied by intracranial hemorrhage. The transverse sinus and superior sagittal sinus with the side walls lack muscle structure and could be compressed by the expanding and swollen parenchyma, leading to obstruction of venous return, and resulting in vasogenic edema.

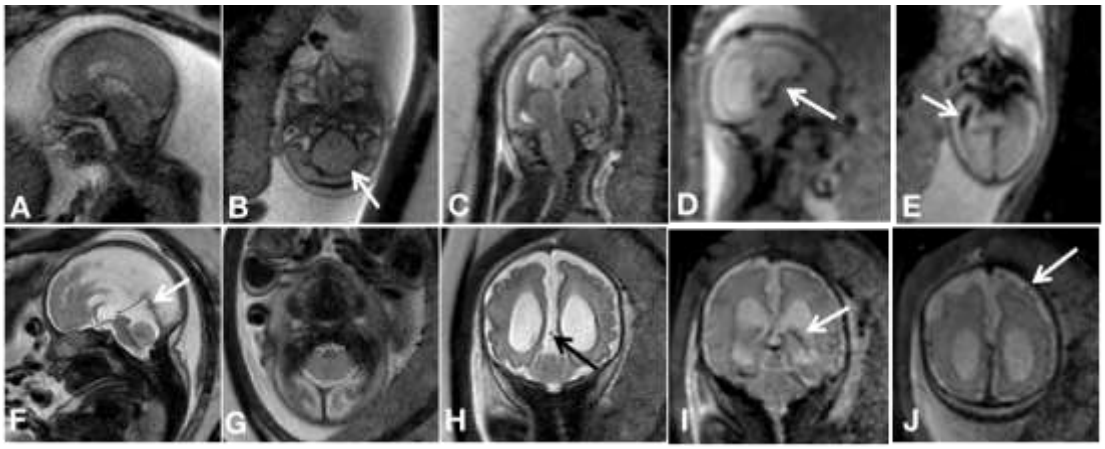

Figure 12: The protective efficacy of intrauterine repair surgery on the venous system.
A-E: MRI of a fetus with Chiari II malformation and brain edema at 21GW, showing almost depleted outer CSF space ("dry" brain), very crowded posterior fossa, and transverse sinus stenosis (arrow), resulting in venous congestion(arrow) and white matter edema, as well as ependyma hemorrhage at the right occipital horn shown on EPI -T2* sequence.
F-J: A follow-up fetal MR exam was performed at 31+4GW after in-utero surgery, which led to an expansion of outer CSF spaces and presumably reestablishment of proper CSF dynamics, and consequently, improved brain edema. It is noteworthy that the hemorrhage disappeared, and the venous system, including both the deep veins and cortical veins, appears to be functioning normally in this follow-up examination.